Characterization of optical properties and surface roughness profiles: The Casimir force between real materials

P. J. van Zwol, V.B. Svetovoy, and G. Palasantzas

Abstract The Lifshitz theory provides a method to calculate the Casimir force between two flat plates if the frequency dependent dielectric function of the plates is known. In reality any plate is rough and its optical properties are known only to some degree. For high precision experiments the plates must be carefully characterized otherwise the experimental result cannot be compared with the theory or with other experiments. In this chapter we explain why optical properties of interacting materials are important for the Casimir force, how they can be measured, and how one can calculate the force using these properties. The surface roughness can be characterized, for example, with the atomic force microscope images. We introduce the main characteristics of a rough surface that can be extracted from these images, and explain how one can use them to calculate the roughness correction to the force. At small separations this correction becomes large as our experiments show. Finally we discuss the distance upon contact separating two rough surfaces, and explain the importance of this parameter for determination of the absolute separation between bodies.

P. J. van Zwol
Materials Innovation Institute and Zernike Institute for Advanced Materials University of Groningen, 9747 AG Groningen, The Netherlands , e-mail: petervanzwol@gmail.com

V. B. Svetovoy
MESA$^+$ Institute for Nanotechnology, University of Twente, PO 217, 7500 AE Enschede, The Netherlands e-mail: v.b.svetovoy@ewi.utwente.nl

G. Palasantzas
Materials Innovation Institute and Zernike Institute for Advanced Materials University of Groningen, 9747 AG Groningen, The Netherlands e-mail: g.palasantzas@rug.nl

1 Introduction

The Casimir force [1] between two perfectly reflecting metals does not depend on the material properties. This is rather rough approximation as the Lifshitz theory demonstrates [2, 3, 4] (see also Dzyaloshinskii and Pitaevskii paper in this volume). In this theory material dependence of the force enters via the dielectric functions of the materials. Because the Casimir-Lifshitz force originates from fluctuations of the electromagnetic field, it is related with the absorption in the materials via the fluctuation dissipation theorem. The dissipation in the material at a frequency ω is proportional to the imaginary part of the dielectric function $\varepsilon(\omega) = \varepsilon'(\omega) + i\varepsilon''(\omega)$. Thus, to predict the force one has to know the dielectric properties of the materials.

In most of the experiments where the Casimir force was measured (see reviews [5, 6] and Lamoreaux paper in this volume) the bodies were covered with conducting films but the optical properties of these films have never been measured. It is commonly accepted that these properties can be taken from tabulated data in handbooks [7, 8]. Moreover, for conducting materials one has to know also the Drude parameters, which are necessary to extrapolate the data to low frequencies [9]. This might still be a possible way to estimate the force, but it is unacceptable for calculations with controlled precision. The reason is very simple [10, 11, 12, 13]: optical properties of deposited films depend on the method of preparation, and can differ substantially from sample to sample.

Analysis of existing optical data for Au [14] revealed appreciable variation of the force in dependence on the optical data used for calculations. Additionally, we measured our gold films using ellipsomety in a wide range of wavelengths $0.14 - 33\,\mu$m [15], and found significant variation of optical properties for samples prepared at different conditions. Considerable dependence of the force on the precise dielectric functions of the involved materials was also stressed for the system solid-liquid-solid [16].

The Lifshitz formula can be applied to two parallel plates separated by a gap d. In reality each plate is rough and the formula cannot be applied directly. When the separation of the plates is much larger than their root-mean-square (rms) roughness w one can calculate correction to the force due to roughness using the perturbation theory. But even in this case the problem is far from trivial [17, 18, 19]. The roughness correction can be easily calculated only if one can apply Proximity Force Approximation (PFA) [20]. Application of this approximation to the surface profile is justified when this profile changes slowly in comparison with the distance between bodies. Typical lateral size of a rough body is given by the correlation length ξ. Then the condition of applicability of PFA is $\xi \gg d$. This is very restrictive condition since, for example, for thermally evaporated metallic films the typical correlation length is $\xi \sim 50$ nm.

The roughness of the interacting bodies restricts the minimal separation d_0 between the bodies. This distance (distance upon contact) has a special significance for adhesion, which under dry conditions is mainly due to Casimir/van der Waals forces across an extensive noncontact area [21]. It is important for micro (nano) electro mechanical systems (MEMS) because stiction due to adhesion is the ma-

jor failure mode in MEMS [22]. Furthermore, the distance upon contact plays an important role in contact mechanics, is very significant for heat transfer, contact resistivity, lubrication, and sealing.

Naively one could estimate this distance as the sum of the rms roughnesses of body 1 and body 2, $d_0 \approx w_1 + w_2$ [23], however, the actual minimal separation is considerably larger. This is because d_0 is determined by the highest asperities rather then those with the rms height. An empirical rule [24] for gold films gives $d_0 \approx 3.7 \times (w_1 + w_2)$ for the contact area of $\sim 1\mu\text{m}^2$. The actual value of d_0 is a function of the size of the contact area L. This is because for larger area the probability to find a very high peak on the surface is larger.

Scale dependence (dependence on the size L) is also important for the Casimir force in the noncontact regime. In this case there is an uncertainty in the separation $\delta d(L)$, which depends on the scale L. The reason for this uncertainty is the local variation of the zero levels, which define the mathematical (average) surfaces of the bodies. This uncertainty depends on the roughness of interacting bodies and disappears in the limit $L \to \infty$.

In this paper we explain how one can collect the information about optical properties of the materials, which is necessary for the calculation of the Casimir-Lifshitz force. It is also discussed how the optical spectra of different materials manifest themselves in the force. We introduce the main characteristics of rough surfaces and discuss how they are related with the calculation of the roughness correction to the force. Scale dependence of the distance upon contact is discussed, and we explain significance of this dependence for the precise measurements of the force.

2 Optical properties of materials and the Casimir force

Most Casimir force measurements were performed between metals [5, 6, 25, 26, 27] either e-beam evaporated or plasma sputtered on substrates. For such metallic films the grains are rather small in the order of tens of nanometers, and the amount of defects and voids is large [28]. The force measured between silicon single crystal and gold coated sphere [29] simplify situation only partly: the optical properties of the Si-crystal are well defined but properties of Au coating are not known well.

A detailed literature survey performed by Pirozhenko et al. [14] revealed significant scatter in the dielectric data of gold films collected by different groups. The measurement errors were not large and could not explain the data scattering. It was concluded that scattering of the data for gold films could lead to uncertainty in the calculated force up to 8% at separations around 100 nm. Most of the optical data for metals do not extend beyond the wavelength of 14 μm in the infrared range [30, 31]. Thus, it would be important to explore more the infrared regime and compare modern measured optical properties of samples used in force measurements with the old data. Moreover, mid and far infrared data are very important for the force prediction (see Sec. 2.2.2). This was accomplished by Svetovoy et al. [15] where ellipsometry from the far infrared (IR) to near ultraviolet (UV) was used over the wavelength

range 140 nm – 33 μm to obtain the frequency dependent dielectric functions for gold films prepared in different conditions. Analysis of different literature sources where the dielectric functions of a number of dielectrics such as silica and some liquids was performed by van Zwol et al. [16]. Situations where the data scattering can change even the qualitative behavior of the force (from attractive to repulsive) were indicated.

2.1 Dielectric function in the Casimir force

In this section we discuss how the dielectric functions of materials enter the Lifshitz theory and how these functions can be found experimentally.

2.1.1 The force

Let us start the discussion from the Lifshitz formula [4] between two parallel plates separated by a gap d. It has the following form

$$F(T,d) = \frac{kT}{\pi}{\sum_{n=0}^{\infty}}' \int_0^{\infty} dqq\kappa_0 \sum_{\nu=s,p} \frac{r_1^\nu r_2^\nu e^{-2\kappa_0 d}}{1-r_1^\nu r_2^\nu e^{-2\kappa_0 d}}, \tag{1}$$

where "prime" at the sign of sum means that the $n=0$ term must be taken with the weight 1/2, the wave vector in the gap is $\mathbf{K}=(\mathbf{q},\kappa_0)$ with the z-component κ_0 defined below. Index "0" is related with the gap. Here $r_{1,2}^\nu$ are the reflection coefficients of the inner surfaces of the plates (index 1 or 2) for two different polarizations: $\nu = s$ or transverse electric (TE) polarization, and $\nu = p$ or transverse magnetic (TM) polarization. Specific of the Lifshitz formula in the form (1) is that it is defined for a discrete set of imaginary frequencies called the Matsubara frequencies

$$\omega_n = i\zeta_n = i\frac{2\pi kT}{\hbar}n, \quad n=0,1,2,..., \tag{2}$$

where T is the temperature of the system and n is the summation index.

In practice the interacting bodies are some substrates covered with one or a few layers of working materials. If the top layer can be considered as a bulk layer then the reflection coefficients for body i are given by simple Fresnel formulas [32]:

$$r_i^s = \frac{\kappa_0-\kappa_i}{\kappa_0+\kappa_i}, \quad r_i^p = \frac{\varepsilon_i(i\zeta)\kappa_0-\varepsilon_0(i\zeta)\kappa_i}{\varepsilon_i(i\zeta)\kappa_0+\varepsilon_0(i\zeta)\kappa_i}, \tag{3}$$

where

$$\kappa_0 = \sqrt{\varepsilon_0(i\zeta)\frac{\zeta^2}{c^2}+q^2}, \quad \kappa_i = \sqrt{\varepsilon_i(i\zeta)\frac{\zeta^2}{c^2}+q^2}. \tag{4}$$

For multilayered bodies these formulas can be easily generalized (in relation with the dispersive forces see Ref. [33]). Only the reflection coefficients depend on the dielectric functions of the plate materials; the function $\varepsilon_0(i\zeta)$ of the gap material enters additionally in κ_0.

At small separations the thermal dependence of the force is very weak and in many cases can be neglected. Because important imaginary frequencies are around the so called characteristic frequency $\zeta_c = c/2d$, then the relative thermal correction can be estimated as $kT/\hbar\zeta_c$. For room temperature $T = 300^\circ$ K and separations smaller than 100 nm the correction will be smaller than 3%. If one can neglect this correction then in the Lifshitz formula ζ can be considered as a continuous variable and the sum in (1) is changed by the integral according to the rule:

$$\frac{kT}{\pi}\sum_{n=0}^{\infty}{}' \to \frac{\hbar}{2\pi^2}\int_0^\infty d\zeta. \tag{5}$$

The material function $\varepsilon(i\zeta)$ (we suppress the indexes for a while) cannot be measured directly but can be expressed via the observable function $\varepsilon''(\omega)$ with the help of the Kramers-Kronig (KK) relation [32]:

$$\varepsilon(i\zeta) = 1 + \frac{2}{\pi}\int_0^\infty d\omega \frac{\omega\varepsilon''(\omega)}{\omega^2+\zeta^2}. \tag{6}$$

The knowledge of $\varepsilon(i\zeta)$ is of critical importance for the force calculations. Equation (6) demonstrates the main practical problem. To find the function $\varepsilon(i\zeta)$ for $\zeta \sim \zeta_c$ in general one has to know the physical function $\varepsilon''(\omega)$ in a wide range of real frequencies, which is not necessary coincides with $\omega \sim \zeta_c$. This property of the Casimir force was stressed in Ref. [12] and then was demonstrated experimentally [34, 35, 36]. It will be discussed below on specific examples.

2.1.2 The optical data

The optical properties of materials are described by two measurable quantities: the index of refraction $n(\lambda)$ and the extinction coefficient $k(\lambda)$, which both depend on the wavelength of the electromagnetic field λ. Combined together they define the complex index of refraction $\tilde{n}(\lambda) = n(\lambda) + ik(\lambda)$. The real part defines the phase velocity in a medium $v = c/n$ where c is the speed of light. The imaginary part tells us how much light is adsorbed when it travels through the medium. The dielectric response of a material for the UV ($\hbar\omega > 5$ eV), IR ($0.01 - 1$ eV) and MicroWave (MW) or TeraHertz range ($10^{-4} - 10^{-2}$ eV), is related to electronic polarization resonances, atomic polarization resonances (in case of metals this is a gas of quasi free electrons), and dipole relaxation, respectively.

The complex dielectric function $\varepsilon(\omega) = \varepsilon'(\omega) + i\varepsilon''(\omega)$ and the complex index of refraction are related as $\varepsilon(\omega) = \tilde{n}^2(\omega)$, which is equivalent to the following equa-

tions:

$$\varepsilon^{'} = n^2 - k^2, \quad \varepsilon^{''} = 2nk. \tag{7}$$

In many cases only the absorbance is measured for a given material. In this case the refraction index can be found from the KK relation at real frequencies:

$$\varepsilon^{'}(\omega) = 1 + \frac{2}{\pi} P \int_0^\infty dx \frac{x\varepsilon^{''}(x)}{x^2 - \omega^2}, \tag{8}$$

where P means the principal part of the integral.

Kramers-Kronig relations originating from causality have a very general character. They are useful in dealing with experimental data, but one should be careful since in most cases dielectric data are available over limited frequency intervals. As a result specific assumptions must be made about the form of the dielectric data outside of measurement intervals, or the data should be combined with other (tabulated) experimental data before performing the KK integrals.

A powerful method to collect optical data simultaneously for both $\varepsilon^{'}$ and $\varepsilon^{''}$ is ellipsomery. This is a non destructive technique where one measures an intensity ratio between incoming and reflected light and the change of the polarization state. Ellipsometry is less affected by intensity instabilities of the light source or atmospheric absorption. Because the ratio is measured no reference measurement is necessary. Another advantage is that both real and imaginary parts of the dielectric function can be extracted without the necessity to perform a Kramers-Kronig analysis. The ellipsometry measures two parameters Ψ and Δ, which can be related to the ratio of complex Fresnel reflection coefficients for p- and s-polarized light [37, 38]

$$\rho = \frac{r^p}{r^s} = \tan\Psi e^{i\Delta}, \tag{9}$$

where $r^{p,s}$ are the reflection coefficients of the investigated surface, and the angles Ψ and Δ are the raw data collected in a measurement as functions of the wavelength λ. When the films are completely opaque (bulk material), then the reflection coefficients are related with the dielectric function as follows

$$r_p = \frac{\langle\varepsilon\rangle\cos\vartheta - \sqrt{\langle\varepsilon\rangle - \sin^2\vartheta}}{\langle\varepsilon\rangle\cos\vartheta + \sqrt{\langle\varepsilon\rangle - \sin^2\vartheta}}, \quad r_s = \frac{\cos\vartheta - \sqrt{\langle\varepsilon\rangle - \sin^2\vartheta}}{\cos\vartheta + \sqrt{\langle\varepsilon\rangle - \sin^2\vartheta}}, \tag{10}$$

where ϑ is the angle of incidence and $\langle\varepsilon\rangle = \langle\varepsilon(\lambda)\rangle$ is the "pseudo" dielectric function of the films. The term "pseudo" is used here since the films may not be completely isotropic or uniform; they are rough, and may contain absorbed layers of different origin because they have been exposed to air. If this is the case then the dielectric function extracted from the raw data will be influenced by these factors. The dielectric function is connected with the ellipsometric parameter ρ for an isotropic and uniform solid as

$$\varepsilon = \sin^2\vartheta\left[1+\tan^2\vartheta\left(\frac{1-\rho}{1+\rho}\right)^2\right]. \tag{11}$$

As it was stated before the spectral range of our measured data is from 137 nm to 33 μm. Even longer wavelengths have to be explored to predict the force between metals without using the extrapolation. Ellipsometry in the terahertz range $0.1-8$ THz (wavelengths $38-3000$ μm) is difficult due to lack of intense sources in that range, and these systems are still in development [39]. Typically synchrotron radiation is used as a source deeming these measurements very expensive. Nonetheless for gold films it would be extremely interesting to have dielectric data in this regime.

Dielectric data obtained by ellipsometry or absorption measurements [40] in the far UV regime are also rare. The most obvious reason for this is that these measurements are expensive because high energy photons must be produced, again at synchrotrons [41]. Furthermore, ellipsometry in this range becomes complicated as polarizing materials become non transparent. For this range a few ellipsometry setups exist around the world covering the range $5-90$ eV (wavelengths $12-200$ nm) [41]. The vacuum UV (VUV) and extreme UV (XUV) parts may not be very important for metals but for low permittivity dielectrics such as all liquids, and, for example, silica or teflon, there is a major absorption band in the range $5-100$ eV (see Fig. 6). It is precisely this band that dominates in the calculations of the Casimir force for these materials. It is very unfortunate that precisely for this band dielectric data are lacking for most substances except for a few well know cases as, for example, water.

2.2 Gold films

In this section we discuss optical characterization of our gold films prepared in different conditions using ellipsometers. Then we discuss the dielectric function at imaginary frequencies for Au films and for metals in general stressing the importance of very low real frequencies for precise evaluation of $\varepsilon(i\zeta)$ at $\zeta \sim \zeta_c \sim 1$ eV (separations around 100 nm). Finally we describe variation in the Casimir force if different samples would be used for the force measurements.

2.2.1 $\varepsilon(\omega)$ for Au films

Let us have now a closer look at the dielectric functions of our gold films [15] used for the force measurements in Refs. [42, 24]. For optical characterization we have prepared five films by electron beam evaporation. Three of these films of different thicknesses 100, 200 and 400 nm were prepared within the same evaporation system on Si with 10 nm titanium sublayer and were not annealed. Different evaporation system was used to prepare two other films. These films were 120 nm thick. One film

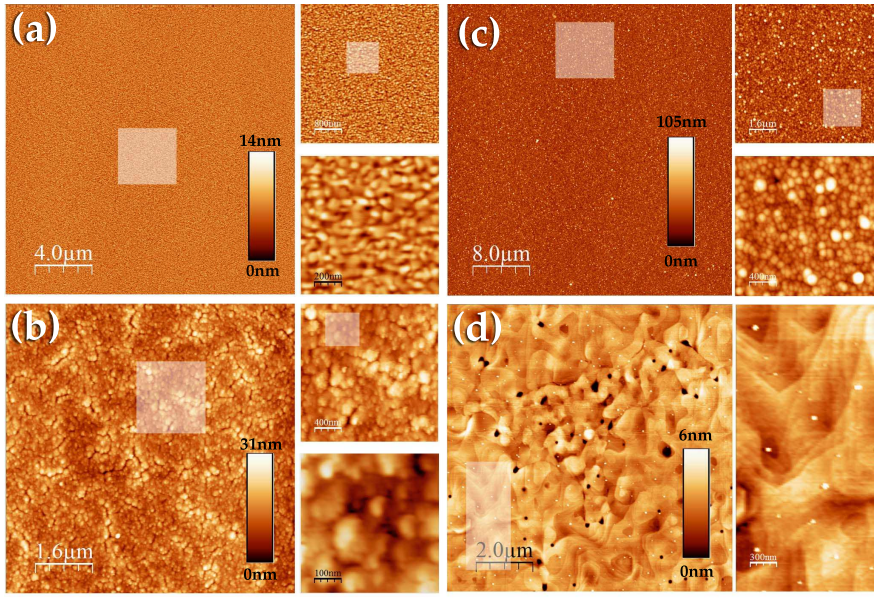

Fig. 1 Flattened roughness scans (up to 4000×4000 pixels) of gold surfaces where the highlighted areas are magnified. The color scale bars can be applied only to the large images. (a) 100 nm Au on Si, (b) Au coated polysterene sphere (first plasma sputtered then 100 nm Au evaporated, (c) 1600 nm Au on Si, (d) very high quality 120 nm Au on mica, annealed for a few hours and slowly cooled down.

was deposited on mica and was extensively annealed. The other one was deposited on Si with chromium sublayer and was not annealed.

The AFM scans of the 100 nm film and the annealed 120 nm film on mica are shown in Fig. 1. In the same figure are shown also the gold covered sphere and 1600 nm film, which where not used in optical characterization. One can see that the annealed sample is atomically smooth over various length scales with atomic steps and terraces visible. Nevertheless, the local trenches of 5 nm deep are still present.

Optical characterization of the films was performed by J. A. Woollam Co., Inc. [43]. Vacuum ultraviolet variable angle spectroscopic ellipsometer (VASE) was used in the spectral range $137 - 1698$ nm. In the spectral range $1.9 - 32.8\,\mu$m the infrared variable angle spectroscopic ellipsometer (IR-VASE) was used for two incidence angle of 65° and 75°. The roughness and possible absorbed layer on the film surface can have some significance in the visible and ultraviolet ranges but not in the infrared, where the absorption on free electrons of metals is very large. Moreover, the effect of roughness is expected to be small since for all films the rms roughness is much smaller than the smallest wavelength 137 nm. Because the infrared domain is the most important for the Casimir force between metals, we will consider $\langle \varepsilon(\lambda) \rangle$ extracted from the raw data as a good approximation for the dielectric function of a given gold film.

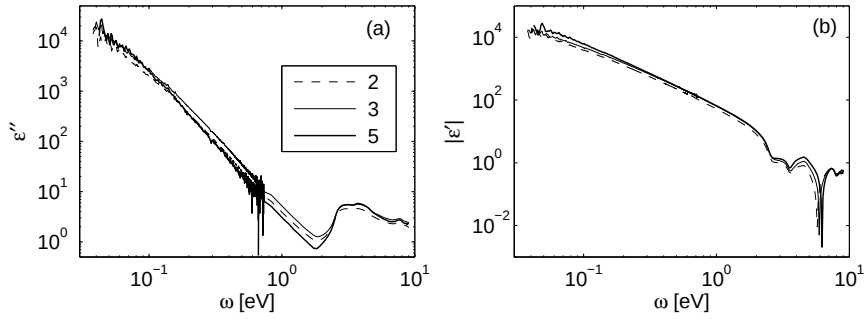

Fig. 2 (a) Measured ε'' as a function of frequency ω. (b) The same for $|\varepsilon'|$. For clearness the results are presented only for three samples 2, 3, and 5.

Figure 2(a) shows the experimental results for $\varepsilon^{''}(\omega)$ for three of five investigated samples. Around the interband transition (minimum of the the curves) the smallest absorption is observed for the sample 5 (annealed on mica) indicating the smallest number of defects in this sample [28]. On the contrary, this sample shows the largest $|\varepsilon^{'}(\omega)|$ in the infrared as one can see in Fig. 2b. An important conclusion that can be drawn from our measurements is the sample dependence of the dielectric function. The sample dependence can be partly attributed to different volumes of voids in films as was proposed by Aspnes *et al.* [28]. The values of ε and their dispersion for different samples are in good correspondence with old measurements [30, 31]. The log-log scale is not very convenient for having an impression of this dependence. We present in Table I the values of ε for all five samples at chosen wavelengths $\lambda = 1, 5, 10\ \mu$m. One can see that the real part of ε varies very significantly from sample to sample.

Sample	$\lambda = 1\ \mu$m	$\lambda = 5\ \mu$m	$\lambda = 10\ \mu$m
1, 400 nm/Si	$-29.7 + i2.1$	$-805.9 + i185.4$	$-2605.1 + i1096.3$
2, 200 nm/Si	$-31.9 + i2.3$	$-855.9 + i195.8$	$-2778.6 + i1212.0$
3, 100 nm/Si	$-39.1 + i2.9$	$-1025.2 + i264.8$	$-3349.0 + i1574.8$
4, 120 nm/Si	$-43.8 + i2.6$	$-1166.9 + i213.9$	$-3957.2 + i1500.1$
5, 120 nm/mica	$-40.7 + i1.7$	$-1120.2 + i178.1$	$-4085.4 + i1440.3$

Table 1 Dielectric function for different samples at fixed wavelengths $\lambda = 1, 5, 10\ \mu$m.

One could object that the real part of ε does not play role for $\varepsilon(i\zeta)$ and only variation of $\varepsilon^{''}(\omega)$ from sample to sample is important. However, both $\varepsilon^{''}(\omega)$ and $\varepsilon^{'}(\omega)$ are important for precise determination of the Drude parameters. Let us discuss now how one can extract these parameters from the data.

All metals have finite conductivity. It means that at low frequencies $\omega \to 0$ the dielectric function behaves as $\varepsilon(\omega) \to 4\pi\sigma/\omega$, where σ is the material conductivity.

It has to be stressed that this behavior is a direct consequence of the Ohm's law and, therefore, it has a fundamental character. Because the dielectric function has a pole at $\omega \to 0$, the low frequencies will give a considerable contribution to $\varepsilon(i\zeta)$ even if ζ is high (for example, in visible part of the spectrum) as one can see from Eq.(6).

Usually it is assumed that at low frequencies the dielectric functions of good metals follow the Drude model:

$$\varepsilon(\omega) = 1 - \frac{\omega_p^2}{\omega(\omega + i\gamma)}, \tag{12}$$

where ω_p is the plasma frequency and γ is the relaxation frequency of a given metal. When $\omega \to 0$ we reproduce the $1/\omega$ behavior with the conductivity $\sigma = \omega_p^2/4\pi\gamma$. For good metals such as Au, Ag, Cu, Al typical values of the Drude parameters are $\omega_p \sim 10^{16}$ rad/s and $\gamma \sim 10^{14}$ rad/s.

Separating real and imaginary parts in Eq. (12) one finds for ε' and ε''

$$\varepsilon'(\omega) = 1 - \frac{\omega_p^2}{\omega^2 + \gamma^2}, \quad \varepsilon''(\omega) = \frac{\omega_p^2 \gamma}{\omega(\omega^2 + \gamma^2)}. \tag{13}$$

These equations can be applied below the interband transition $\omega < 2.45$ eV ($\lambda > 0.5\ \mu$m) [44], but this transition is not sharp and one has to do analysis at lower frequencies. Practically Eq. (13) can be applied at wavelengths $\lambda > 2\ \mu$m that coincides with the range of the infrared ellipsometer. The simplest way to find the Drude parameters is to fit the experimental data for ε' and ε'' with both equations (13). Alternatively to find the Drude parameters one can use the functions $n(\omega)$ and $k(\omega)$ and their Drude behavior, which follows from the relation $\varepsilon(\omega) = \tilde{n}^2(\omega)$. This approach uses actually the same data but weight noise differently.

Completely different but more complicated approach is based on the KK relations (8) (see Refs. [14] and [15] for details). In this case one uses measured $\varepsilon''(\omega)$ extrapolated to low frequencies according to the Drude model and extrapolated to high frequencies as A/ω^3, where A is a constant. In this way we will get $\varepsilon''(\omega)$ at all frequencies. Using then Eq. (8) we can predict $\varepsilon'(\omega)$. Comparing the prediction with the measured function we can determine the Drude parameters. Similar procedure can be done for $n(\omega)$ and $k(\omega)$.

	1, 400 nm/Si	2, 200 nm/Si	3, 100 nm/Si	4, 120 nm/Si	5, 120 nm/mica
γ (meV)	40.5 ± 2.1	49.5 ± 4.4	49.0 ± 2.1	35.7 ± 5.1	37.1 ± 1.9
ω_p (eV)	6.82 ± 0.08	6.83 ± 0.15	7.84 ± 0.07	8.00 ± 0.16	8.38 ± 0.08
ξ (nm)	22	26	32	70	200
w (nm)	4.7	2.6	1.5	1.5	0.8

Table 2 Drude parameters γ, ω_p and roughness parameters, the correlation length ξ and rms roughness w, for all five measured samples.

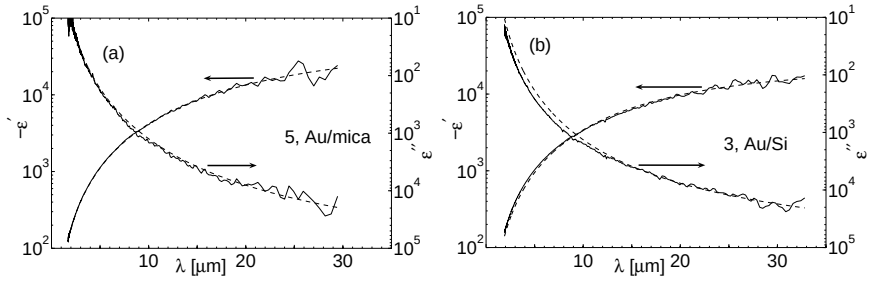

Fig. 3 The infrared data as functions of the wavelength λ for ε' and ε'' (solid lines) and the best Drude fits (dashed lines) for two gold films. Panel (a) shows the data for annealed sample 5 and panel (b) shows the same for unannealed sample 3.

All methods for determination of the Drude parameters give reasonably close values of both parameters. We cannot give preference to any specific method. Instead, we average the values of the parameters determined by different methods, and define the rms error of this averaging as uncertainty in the parameter value. The averaged parameters and rms errors are given in the Table 2. We included in this table also the correlation lengths ξ and the rms roughness w for the sample roughness profiles. One can see the ω_p and ξ correlate with each other [1]. This correlation has sense because ξ describes the average size of the crystallites in the film; the larger the crystallites the smaller number of the defects has the film and, therefore, the larger value of the plasma frequency is realized.

Quality of the Drude fit one can see in Fig. 3 for samples 3 and 5. The fit is practically perfect for high quality sample 5, but there are some deviations for sample 3 at short wavelengths especially visible for ε''. More detailed analysis [15] revealed presence of a broad absorption peak of unknown nature around $\lambda = 10\ \mu$m. The magnitude of this absorption is the largest for poor quality samples 1 and 2.

2.2.2 $\varepsilon(i\zeta)$ for metals

Any method of optical characterization has a minimal accessible frequency ω_{cut} (cut-off frequency). At $\omega > \omega_{cut}$ one can measure the dielectric function but at lower frequencies $\omega < \omega_{cut}$ one has to make an assumption on the behavior of $\varepsilon(\omega)$, i. e. extrapolate to low frequencies. In KK relation (6) one can separate two intervals: $\omega < \omega_{cut}$, where $\varepsilon''(\omega)$ has to be extrapolated and $\omega > \omega_{cut}$, where $\varepsilon''(\omega)$ is measured. Then we can present $\varepsilon(i\zeta)$ as

$$\varepsilon(i\zeta) = 1 + \varepsilon_{cut}(i\zeta) + \varepsilon_{exper}(i\zeta),$$

[1] This correlation was not noted in [15] and stressed here for the first time.

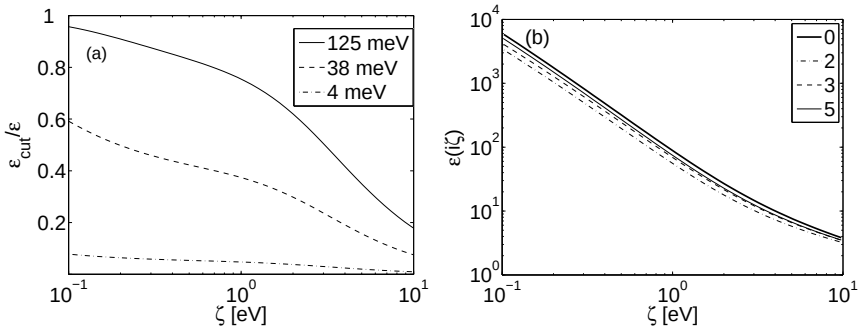

Fig. 4 (a) Relative contribution $\varepsilon_{cut}(i\zeta)/\varepsilon(i\zeta)$ to the dielectric function of gold at imaginary frequencies originating from the extrapolated region $\omega < \omega_{cut}$ (see explanations in the text). (b) The dielectric functions at imaginary frequencies for samples 2,3, and 5; the thick curve marked as 0 corresponds to an "ideal sample" with the plasma frequency of single crystal.

$$\varepsilon_{cut}(i\zeta) = \frac{2}{\pi}\int_0^{\omega_{cut}} d\omega \frac{\omega\varepsilon''(\omega)}{\omega^2+\zeta^2}, \quad \varepsilon_{exper}(i\zeta) = \frac{2}{\pi}\int_{\omega_{cut}}^{\infty} d\omega \frac{\omega\varepsilon''(\omega)}{\omega^2+\zeta^2}. \tag{14}$$

Of course, at very high frequencies we also do not know $\varepsilon''(\omega)$ but, for metals high frequencies are not very important. For this reason we include the high frequency contribution to $\varepsilon_{exper}(i\zeta)$.

We can estimate now the contribution of $\varepsilon_{cut}(i\zeta)$ to $\varepsilon(i\zeta)$. For that we assume the Drude behavior at $\omega < \omega_{cut}$ with the parameters $\omega_p = 9.0$ eV and $\gamma = 35$ meV [9]. At higher frequencies $\omega > \omega_{cut}$ we take the data from the handbook [7], for which the cut-off frequency is $\omega_{cut} = 0.125$ eV. These extrapolation and data were used for interpretation most of the experiments, where the Casimir force was measured. In Fig. 4(a) the solid curve is the ratio $\varepsilon_{cut}(i\zeta)/\varepsilon(i\zeta)$ calculated with these data. One can see that at $\zeta = 1$ eV ($d \sim 100$ nm) the contribution to $\varepsilon(i\zeta)$ from the frequency range $\omega < \omega_{cut}$ is 75%. It means, for example, that if we change the Drude parameters, three fourths of $\varepsilon(i\zeta)$ will be sensitive to this change and only one forth will be defined by the measured optical data. Therefore, the extrapolation procedure becomes very important for reliable prediction of $\varepsilon(i\zeta)$.

The Drude parameters can vary from sample to sample due to different density of defects. The plasma frequency is related with the density of quasifree electrons N as $\omega_p^2 = 4\pi N e^2/m_e^*$, where for gold $m_e^* \approx m_e$ is the effective mass of electron. The value $\omega_p = 9.0$ eV is the maximal value of this parameter, which corresponds to N in a single crystal Au. In this way ω_p was estimated in Ref. [9]. All deposited films have smaller values of ω_p as one can see from Tab. 2 because the density of the films is smaller than that for the single crystal material. Precise values of the Drude parameters are extremely important for evaluation of $\varepsilon(i\zeta)$ and finally for calculation of the force.

The dielectric function $\varepsilon(i\zeta)$ becomes less dependent on the Drude parameters if the cut-off frequency is smaller. For example, our optical data [15] were collected

up to minimal frequency $\omega_{cut} = 38$ meV that is about four times smaller than in the handbook data. The dashed curve in Fig. 4(a) shows the ratio $\varepsilon_{cut}/\varepsilon$ calculated for our sample 3 with the Drude parameters $\omega_p = 7.84$ eV and $\gamma = 49$ meV. Now the relative contribution of $\varepsilon_{cut}(i\zeta)$ at $\zeta = 1$ eV is 37%. It is much smaller than for handbook data, but still dependence on the precise Drude parameters is important. Let us imaging now that we have been able to measure the dielectric response of the material for the same sample 3 from [15] to frequencies as low as 1 THz. In this case the cut-off frequency is $\omega_{cut} = 4$ meV and the relative contribution of the extrapolated region $\varepsilon_{cut}/\varepsilon$ is shown in Fig. 4(a) by the dash-dotted line. Now this contribution is only 5% at $\zeta = 1$ eV.

The dielectric functions $\varepsilon_i(i\zeta)$, where $i = 1, 2, .., 5$ is the number of the sample, were calculated using the Drude parameters from Tab. 2. As a reference curve we use $\varepsilon_0(i\zeta)$, which was evaluated with the parameters $\omega_p = 9.0$ eV and $\gamma = 35$ meV in the range $\omega < 0.125$ eV and at higher frequencies the handbook data [7] were used. The results are shown in Fig. 4(b). As was expected the maximal dielectric function is $\varepsilon_0(i\zeta)$, which corresponds in the Drude range to a perfect single crystal. Even for the best sample 5 (annealed film on mica) the dielectric function is 15% smaller than $\varepsilon_0(i\zeta)$ at $\zeta = 1$ eV. For samples 1 and 2 the deviations are as large as 40%.

2.2.3 The force between Au films

It is convenient to calculate not the force itself but so called the reduction factor η, which is defined as the ratio of the force to the Casimir force between ideal metals:

$$\eta(d) = \frac{F(d)}{F^c(d)}, \quad F^c(d) = -\frac{\pi^2 \hbar c}{240 d^4}. \tag{15}$$

We calculate the force between similar materials at $T = 0$ using the substitute (5) in Eq. (1). For convenience of the numerical procedure one can make an appropriate change of variables so that the reduction factor can be presented in the form

$$\eta(d) = \frac{15}{2\pi^4} \sum_{\mu=s,p} \int_0^1 dx \int_0^\infty \frac{dy y^3}{r_\mu^{-2} e^y - 1}, \tag{16}$$

where the reflection coefficients as functions of x and y are defined as

$$r_s = \frac{1-s}{1+s}, \quad r_p = \frac{\varepsilon(i\zeta_c xy) - s}{\varepsilon(i\zeta_c xy) + s}, \tag{17}$$

with

$$s = \sqrt{1 + x^2 [\varepsilon(i\zeta_c xy) - 1]}, \quad \zeta_c = \frac{c}{2d}. \tag{18}$$

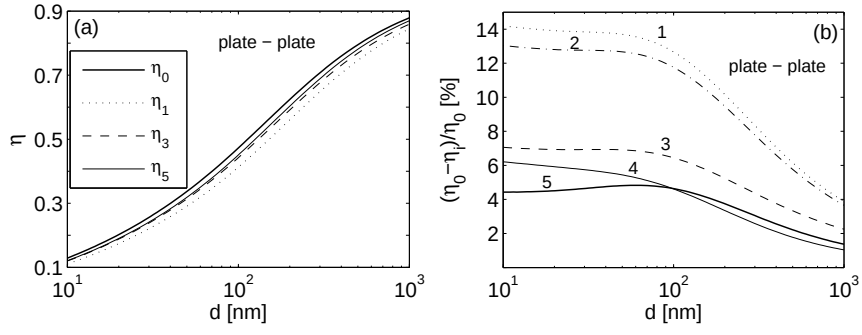

Fig. 5 (a) Reduction factor η as a function of the separation d for samples 1, 3, and 5. The thick line shows the reference result calculated with $\varepsilon_0(i\zeta)$. (b) Relative deviations of the reduction factors for different samples from the reference curve $\eta_0(d)$, which were evaluated using the handbook optical data [7] and the Drude parameters $\omega_p = 9$ eV, $\omega_\tau = 35$ meV.

The integral (16) was calculated numerically with different dielectric functions $\varepsilon_i(i\zeta)$. The results are presented in Fig. 5(a) for samples 1, 3, and 5. The reference curve (thick line) calculated with $\varepsilon_0(i\zeta)$ is also shown for comparison. It represents the reduction factor, which is typically used in the precise calculations of the Casimir force between gold surfaces. One can see that there is significant difference between this reference curve and those that correspond to actual gold films. To see the magnitude of the deviations from the reference curve, we plot in Fig. 5(b) the ratio $(\eta_0 - \eta_i)/\eta_0$ as a function of distance d for all five samples.

At small distances the deviations are more sensitive to the value of ω_p. At large distances the sample dependence becomes weaker and more sensitive to the value of ω_τ. For samples 1 and 2, which correspond to the 400 nm and 200 nm films deposited on Si substrates, the deviations are especially large. They are 12-14% at $d < 100$ nm and stay considerable even for the distances as large as 1 μm. Samples 3, 4, and 5 have smaller deviations from the reference case but even for these samples the deviations are as large as 5-7%.

2.3 Low dielectric materials

The Lifshitz theory predicts [3] that the dispersive force can be changed from attractive to repulsive by choosing the interacting materials immersed in a liquid. Recently this prediction was confirmed experimentally [45] (see Capasso paper in this volume). Repulsive forces arise when the dielectric functions at imaginary frequencies in the liquid gap, $\varepsilon_0(i\zeta)$, is in between the functions of the interacting bodies 1 and 2: $\varepsilon_1(i\zeta) > \varepsilon_0(i\zeta) > \varepsilon_2(i\zeta)$. One can expect significant dependence on precise dielectric functions nearby the transition from attractive to repulsive force. This situation is exactly the case for the system silica-liquid-gold. In this section we present

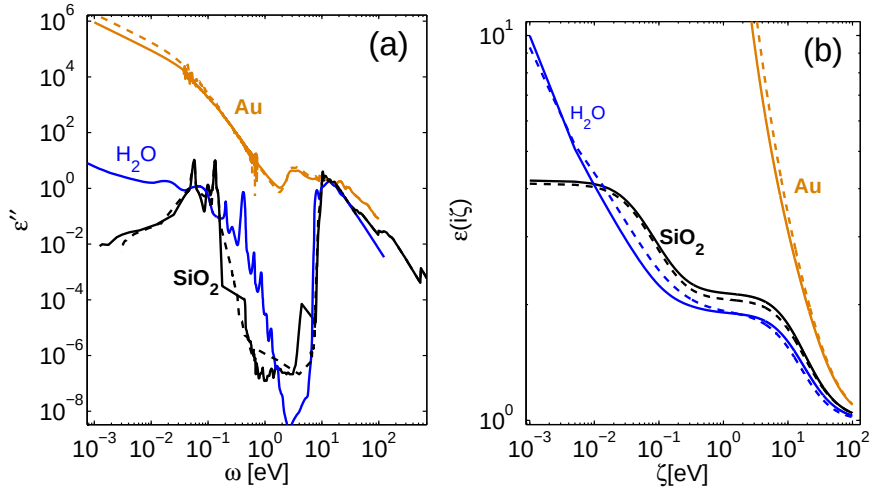

Fig. 6 (a) Dielectric data of the materials obtained from references in text. (b) Dielectric functions at imaginary frequencies. The solid and dashed lines for silica and gold are two different sets of optical data. For water the solid line is from the data in Ref. [49], and the dashed line is an 11-order oscillator model [50], which has been fitted to a different set of optical data.

calculations for multiple liquids with various degrees of knowledge of the dielectric functions.

Liquids do not have grains or defects, but the density of a liquid is a function of temperature [46], and as a result the number of absorbers in the liquid varies with temperature. Furthermore, liquids can contain impurities like salt ions which can change the dielectric function (see discussion in Ref. [47]). Although for metals the dielectric function is very large in the IR regime, for liquids and glasses it is not the case. Consequently for low dielectric materials the UV and VUV dielectric data have a strongest effect on the forces.

For gold, silica, and water the dielectric functions are well known and measured by various groups. Let us consider first the interaction in the system gold-water-silica. We will use two sets of data for gold from the previous subsection (sample 1 and the "ideal sample"). Also two sets of data will be used for silica as obtained by different groups [48]. Finally, for water we will use the data of Segelstein compiled from different sources [49], and an 11-order oscillator model [50] that has been fit to different sets of data [51, 52]. All the dielectric data are collected in Fig. 6(a). The corresponding functions at imaginary frequencies are shown in Fig. 6(b). One can see considerable difference between solid and dashed curves corresponding to different sets of the data.

It has to be noted that $\varepsilon''(\omega)$ for water and silica are very close in a wide range of frequencies $5 \cdot 10^{-2} < \omega < 5 \cdot 10^{2}$ eV. As the result at imaginary frequencies $\varepsilon_{SiO_2}(i\zeta)$ and $\varepsilon_{H_2O}(i\zeta)$ differ on 30% or less in the range $10^{-2} < \zeta < 10^{2}$ eV, which

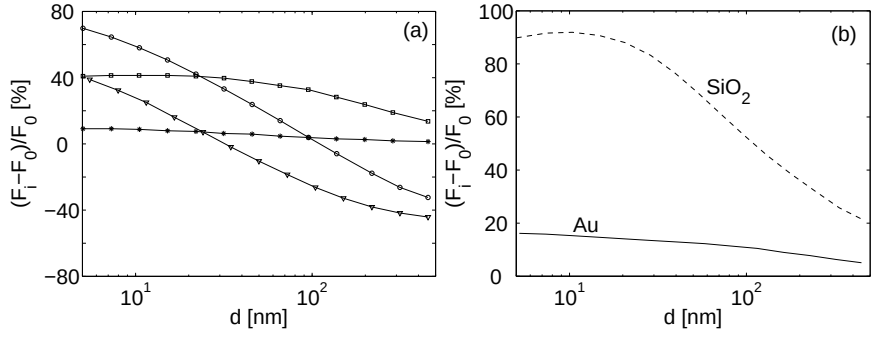

Fig. 7 (a) Variation of the force relative to $F_0(d)$ in the system gold-water-silica. Circles, squares, triangles and stars mark the curves which were calculated using different sets of the dielectric data. (b) Variation of the force for silica-water-silica (dashed line) with different sets of data for SiO_2 and for gold-water-gold (solid line) using different data for Au.

is comparable with the magnitude of variation of $\varepsilon(i\zeta)$ due to data scattering. This similarity in the dielectric functions results in a strong dependence of the Casimir force in the system gold-water-silica on the used optical data. It is illustrated in Fig. 7(a) where the relative change of the force is shown. The scatter of the force riches of the level of 60% for separation $d < 500$ nm. Even more clear the effect can be seen in Fig. 7(b). The solid curve shows variation of the force in Au-water-Au system when different optical data for Au are used. In this case the relative change of the force is not very large. However, for the system silica-water-silica the use of different optical data for silica influence the force very significantly (dashed curve).

We have to conclude that comparison of force measurements with prediction of the Lifshitz theory becomes reliable when the dielectric properties of the specific samples used in force measurement are measured over a wide range of frequencies.

In most of the papers where liquid gap between bodies is studied the dielectric function of the liquid is approximated using the oscillator models [53, 54]. For illustration purposes we mention that alcohols (and other liquid substances) can be described, for example, by a three oscillator model for the dielectric function $\varepsilon(i\zeta)$ at imaginary frequencies [53]

$$\varepsilon(i\zeta) = 1 + \frac{\varepsilon_0 - \varepsilon_{IR}}{1+\zeta/\omega_{MW}} + \frac{\varepsilon_{IR} - n_0^2}{1+(\zeta/\omega_{IR})^2} + \frac{n_0^2 - 1}{1+(\zeta/\omega_{UV})^2}. \tag{19}$$

Here n_0 is the refractive index in the visible range, ε_0 is the static dielectric constant, and ε_{IR} is the dielectric constant where MW relaxation ends and IR begins. The parameters ω_{MW}, ω_{IR}, and ω_{UV} are the characteristic frequencies of MW, IR, and UV absorption, respectively. It has to be stressed that oscillator models should be used with caution, because some of them are of poor quality [16].

For ethanol rather detailed information on the dielectric function exists, but even in this case variation in dielectric data was found [16, 40]. An interesting fact for

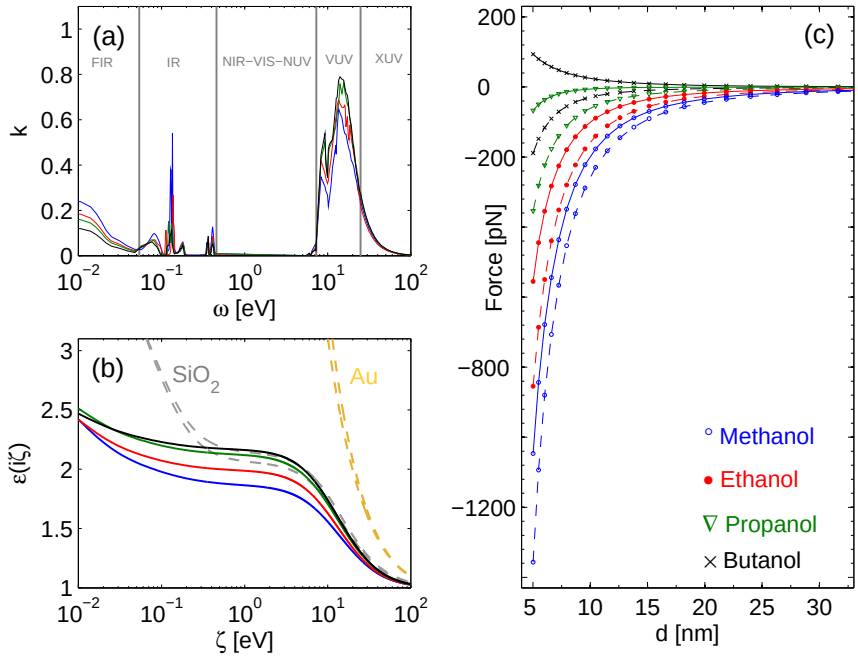

Fig. 8 Dielectric data at real (a) and at imaginary frequencies (b) for methanol, ethanol, propanol, and butanol, as described in the text. For comparison the dielectric data for silica and gold samples are also shown in (b). In (c) we show the forces for the gold-alcohol-silica, for two different sets of measured dielectric data for silica. In the case of butanol the force is attractive for one set, and repulsive for another one.

higher alcohols is that the absorption in the UV range increases when increasing the alkane chain. In Fig. 8 we show the dielectric data for the first four alcohols.

The VUV data were taken from [55]. These measurements were done in the gas phase, but they can be converted to the liquid case by considering the number of absorbers in gas and liquid. The near UV data was taken from [56]. For the XUV we have only data for ethanol and propanol [57]. For methanol and butanol we used cubic extrapolation, $\varepsilon'' \sim 1/\omega^3$, which is in very good agreement with the cases of ethanol and propanol. In the near IR (NIR) to visible (VIS) ranges the extinction coefficient k of ethanol, and other alcohols, is very low and can be taken to be zero, $k = 0$, which is qualitatively consistent with the fact that all alcohols are transparent in the visible range. The IR data can be found in Ref. [58]. The far IR (FIR) data are known only for methanol [59]. For the other alcohols we take the similar functional behavior as for methanol but with different parameters and extrapolate the data to far IR in this way.

If one has to estimate the dielectric functions for some alcohols, first of all one has to have measured data in the range of major IR peaks and even more impor-

tantly the UV absorption must be carefully measured. Thus the dielectric functions at imaginary frequencies should be reasonably accurate to within the scatter of the data as it was found for ethanol [40].

With the optical data for alcohols we calculated the forces in the system gold-alcohol-silica. The forces are attractive and become weaker for methanol, ethanol and propanol. For butanol they are extremely weak, but still either repulsive or attractive. Caution is required in the analysis of optical properties in liquids since in general the KK consistency has to be applied properly in order to correct for variation of the dielectric properties observed in between different measuring setups. Effectively the force for gold-butanol-silica is screened to within the scatter of the forces related to sample dependence of the optical properties of silica. Measurements between gold and glass with simple alcohols were performed, but experimental uncertainty, and double layer forces prevented the measurement of this effect [60].

3 Influence of surface roughness on the Casimir-Lifshitz force

The Lifshitz formula (1) does not take into account inevitable roughness of the interacting bodies. When rms roughness of the bodies is much smaller than the separation, then the roughness influence on the force can be calculated using the perturbation theory [17, 18, 19]. However, when the separation becomes comparable with the roughness the perturbation theory cannot be applied. It was demonstrated experimentally [24] that in this regime the force deviates significantly from any theoretical prediction. The problem of short separations between rough bodies is one of the unresolved problems. In this section we give introduction into interaction of two rough plates and a sphere and a plate.

3.1 Main characteristics of a rough surface

Suppose there is a rough plate which surface profile can be described by the function $h(x,y)$, where x and y are the in-plane coordinates. An approximation for this function provides, for example, an AFM scan of the surface. It gives the height h_{ij} at the pixel position $x_i = \Delta \cdot i$ and $y_j = \Delta \cdot j$, where $i, j = 1,2,...,N$ and Δ is the pixel size related with the scan size as $L = \Delta \cdot N$. We can define the mean plane of the rough plate as the averaged value of the function $h(x,y)$: $\overline{h} = A^{-1} \int dxdyh(x,y)$, where A is the area of the plate. This definition assumes that the plate is infinite. In reality we have to deal with a scan of finite size, for which the mean plane is at

$$h_{av} = \frac{1}{N^2} \sum_{i,j} h(x_i, y_j). \tag{20}$$

The difference $\bar{h} - h_{av}$, although small, is not zero and is a random function of the scan position on the plate. This difference becomes larger the smaller the scan size is. Keeping in mind this point, which can be important in some situations (see below), we can consider (20) as an approximate definition of the mean plane position.

An important characteristic of the a rough surface is the rms roughness w, which is given as

$$w = \frac{1}{N^2} \sum_{i,j} [h(x_i, y_j) - h_{av}]^2 . \tag{21}$$

It has the meaning of the surface width. More detailed information on the rough surface can be extracted from the height-difference correlation function defined for the infinite surface as

$$g(R) = \frac{1}{A} \int dxdy \; [h(\mathbf{r} + \mathbf{R}) - h(\mathbf{r})]^2 , \tag{22}$$

where $\mathbf{r} = (x, y)$ and $\mathbf{R} = \mathbf{r}' - \mathbf{r}$.

A wide variety of surfaces, as for example, deposited thin films far from equilibrium, exhibit the so called self-affine roughness which is characterized besides the rms roughness amplitude w by the lateral correlation length ξ (indicating the average lateral feature size), and the roughness exponent $0 < H < 1$ [61, 62, 63]. Small values of $H \sim 0$ corresponds to jagged surfaces, while large values of $H \sim 1$ to a smooth hill valley morphology. For the self-affine rough surfaces $g(R)$ scales as

$$g(R) = \begin{cases} R^{2H}, \; R \ll \xi , \\ 2w^2, \; R \gg \xi . \end{cases} \tag{23}$$

The parameters w, ξ and H can be determined from the measured height-difference correlation function $g(R)$. This function can be extracted approximately from the AFM scans of the surface.

To find roughness correction to the force one has to know (see below) the spectral density $\sigma(k)$ of the height-height correlation function $C(R)$. The latter is related with $g(R)$ as $g(R) = 2w^2 - C(R)$. An analytic form of the spectral density for a self-affine surface is given by [64]

$$\sigma(k) = \frac{CHw^2\xi^2}{(1 + k^2\xi^2)^{1+H}}, \quad C = \frac{2}{1 - (1 + k_c^2\xi^2)^{-H}} . \tag{24}$$

Here C is a normalization constant [64, 63] and $k_c = 2\pi/L_c$ is the cutoff wavenumber.

3.2 Roughness correction

While the separation between two surfaces is large in comparison with the rms roughness, $d \gg w$, one can use the perturbation approach to calculate the rough-

ness correction to the Casimir force. This correction was calculated first using the proximity force approximation [65]. This approximation assumes that the surface profile slowly varied in comparison with the distance between the bodies. The lateral size of a rough profile is given by the correlation length ξ, therefore, PFA can be applied if $\xi \gg d$. This condition is very restrictive since typical values of ξ for deposited metals films (grain size) are in the range 20-100 nm. In most of the experimental situations the condition $\xi \gg d$ is broken. It was realized for the first time in Ref. [17]. More general theory [17, 18, 19] for the roughness correction can be applied at $\xi \leq d$ and treats the correction perturbatively within the scattering formalism (see Lambrecht paper in this volume). Here we discuss application of this theory to realistic rough surfaces and describe situations, for which one has to go beyond the perturbation theory to find agreement with experiments.

3.2.1 Application of the perturbation theory

Let us consider two parallel rough plates. A plate surface can be described by the roughness profile $h_i(x,y)$ ($i = 1,2$ for plate 1 or 2) as shown in Fig. 9(a). The averaged value over large area is assumed to be zero $\langle h_i(x,y)\rangle = 0$. Then the local distance between the plates is

$$d(x,y) = d - h_1(x,y) - h_2(x,y). \tag{25}$$

This distance depends on the combined rough profile $h(x,y) = h_1(x,y) + h_2(x,y)$. As explained in Sec. 3.3 the interaction of two rough plates is equivalent to the interaction of a smooth plate and a rough plate with the roughness given by the combined profile $h(x,y)$ (see Fig. 9(b)).

Let us assume further that the interaction energy per unit area of two flat plates is $E_{pp}(d)$. If the rms roughness of the combined profile $h(x,y)$ is small, $w \ll d$, but the correlation length is large, $\xi \gg d$, we can present the interaction between rough plates as

$$E_{pp}^{rough} = \left\langle E_{pp}\left(d(x,y)\right)\right\rangle \approx E_{pp}(d) + \frac{E''_{pp}}{2}\left\langle h^2\right\rangle, \tag{26}$$

where $\left\langle h^2\right\rangle = w^2 = w_1^2 + w_2^2$. Equation (27) defines the PFA roughness correction $\delta E_{pp} = E''_{pp} w^2/2$. This correction was used in all early studies to estimate the roughness effect.

It was noted [17] that in most experimental configurations the condition $\xi \gg d$ is broken and PFA cannot be applied. In Refs. [18, 19] was developed a theory, which is not restricted by the condition $\xi \gg d$. Within this theory the roughness correction is expressed via the spectral density of the rough surface $\sigma(k)$ as

$$\delta E_{pp}(d) = \int \frac{d^2k}{(2\pi)^2} G(k,d)\sigma(k), \tag{27}$$

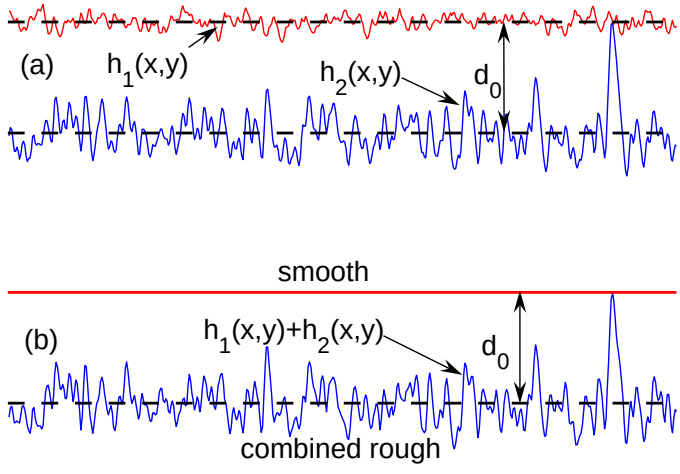

Fig. 9 Contact of two rough surfaces. (a) Two rough plates in contact. Roughness of each plate, $h_i(x,y)$, is counted from the mean plane shown by the dashed line. The distance between bodies is the distance between these mean planes. (b) The interaction between two rough plates is equivalent to the interaction between a smooth plate and a rough plate with the roughness given by the combined profile $h(x,y)$. The distance upon contact, d_0 has well defined meaning in this case. See Sec. 3.3 and Ref. [72] for details.

where $G(k,d)$ is a roughness response function derived in [19]. The PFA result (27) is recovered from here in the limit of small wavenumbers $k \to 0$ when $G(k,d) \to E''_{pp}(d)/2$. The roughness power spectrum is normalized by the condition $\int d^2k\sigma(k)/(2\pi)^2 = w^2$. The spectrum itself can be obtained from AFM scans and in the case of self-affine rough surfaces is given by Eq. (24).

Let us enumerate the conditions at which Eq. (27) is valid. (i) The lateral dimensions of the roughness ξ must be much smaller than the system size L, $\xi \ll L$. This is usually the case in experiments. (ii) The rms roughness w must be small compared to the separation distance, $w \ll d$. This condition means that roughness is treated as perturbative effect. (iii) The lateral roughness dimensions must be much larger than the vertical dimensions, $w \ll \xi$ [19]. The last two assumptions are not always satisfied in the experiment.

In the plate-plate configuration the force per unit area can be calculated as the derivative of $E_{pp}^{rough}(d)$. For the sphere-plate configuration, which is used in most of the experiments, the force is calculated with the help of PFA as $F_{sp}(d) = 2\pi R E_{pp}^{rough}(d)$. In contrast with the roughness correction the latter relation is justified for $d \ll R$, which holds true for most of the experimental configurations. We use the sphere-plate configuration to illustrate the roughness effect. The deposited gold films can be considered as self-affine. For all calculations reported here we are using our smoothest spheres with the parameters $w = 1.8$ nm, $\xi = 22$ nm, and $H = 0.9$. We alter only the plate roughness since it is easy to prepare and replace

during experiments. We use the optical data for gold films described previously. It was found that the PFA limit is quickly recovered for increasing correlation length. Deviations from PFA prediction for real films were found to be about 1-5% in the range $d = 50 - 200$ nm.

Therefore, for real rough surfaces the scattering theory gives a few percent correction to the force compared to the PFA. This difference is difficult to measure. However, at small separations both PFA and perturbation theory fail since the rms roughness becomes comparable in size to the separation distance. It would be interesting to calculate the roughness effect when d is comparable with w. At the moment there is no a theoretical approach to estimate the effect except a direct numerical analysis similar to that used in [66]. It will therefore be interesting to do a full numerical analysis for films with high local slopes instead of using perturbation theory. On the other hand it is experimentally possible to go to sufficiently small distances as it will be discussed below.

3.2.2 Experimental evidence of large roughness effect

The Casimir forces between a 100 μm gold coated sphere and substrates covered with Au to different thicknesses from 100 nm to 1600 nm were measured in [24]. Different layers of Au resulted to different roughnesses and different correlation lengths, which are collected in Tab. 3. The roughness exponent was constant $H = 0.9 \pm 0.05$ in agreement with former growth studies of thin films [64, 62]. The sphere was attached to a cantilever with a spring constant of 0.2 N/m. The calibration procedure is described in [24].

The force results are shown in Fig. 10. Our measurements were restricted to separations below 200 nm where the Casimir force is large enough compared to the approximately linear signal from laser light surface backscattering [26, 24]. The small separation limit or contact point is restricted by the jump to a contact (~ 5 nm) [67, 68, 69] and surface roughness. Note that an error of 1.0 nm in absolute distance leads to errors in the forces of up to 20% at close separations as for example $d \sim 10$ nm [24]. Thus we cannot detect the scattering effects described above. What we do see is the failure of the perturbation theory, for the roughest films, for which the roughness strongly increases the force. These deviations are quite large, resulting in much stronger forces at the small separations < 70 nm. At larger separations, 70-130 nm (within our measurement range), where the roughness influence is negligible, the usual $1/d^{2.5}$ scaling of the force observed also in other experiments with gold is recovered and agreement with the theory is restored. For the smoother films deviations from theory below 40 nm can be explained with the error in the distance.

Qualitatively the roughness effect can be reproduced by calculating the force between small areas on the surfaces separated by the local distance $d(x,y)$. One can call this procedure the non-perturbative PFA approach. Although it is qualitative, it can be used to obtain an estimate of the force at close proximity (2 nm above the point upon contact), where the roughness has an enormous influence on the Casimir force (see inset in Fig. 10). This explains the jump to contact only partially,

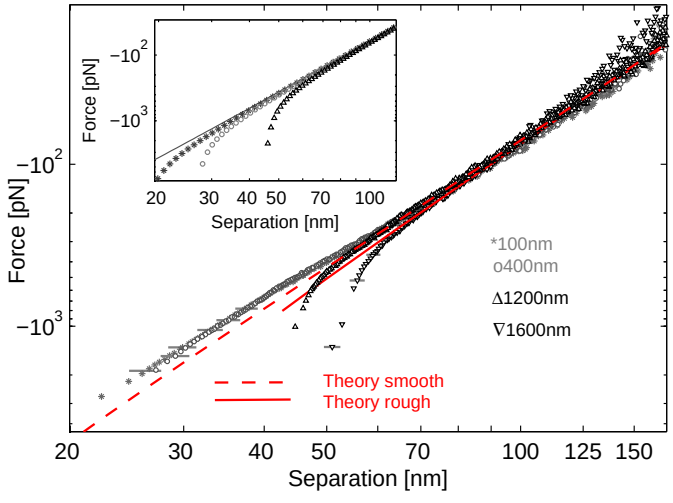

Fig. 10 Casimir forces measured for the films of different roughness. The roughness effect manifests itself as a strong change in scaling at smaller separations, where the forces become much stronger. Errors in separation are shown for some points by the horizontal bars. The theoretical curves are shown for the 100 nm (smooth) and 1600 nm (rough) films. The inset shows the forces calculated by integrating over the roughness scans using PFA (see text).

since approximately 5 nm above the point of contact, the capillary force will act as well. This force appears due to absorbed water and Kelvin condensation [70, 22] resulting in water bridges formation between bodies. In the limit of fully wetted surface (see Fig. 11) the capillary force is given by $F_{cap} \approx 4\pi\gamma R\cos\vartheta$ (upper dashed line), while for a single asperity (of size ξ) wetting the minimum capillary force is $F_{cap} \approx 4\pi\gamma\xi\cos\vartheta$ (lower dashed line). Here γ is the surface tension of liquid, and ϑ is the contact angle [69, 67].

At this point we have to compare the Casimir adhesion between rough films with adhesion by capillary forces [68, 69]. While Casimir forces may lead to stiction between movable parts, once the surfaces are in contact capillary forces (being present in air between hydrophilic surfaces into close proximity) are much stronger. The roughness effect on capillary adhesion is also much stronger as shown in Fig. 11. Note that the Casimir force for a $R = 50\,\mu$m sphere is in the order of 10 nN at 10 nm separations. Capillary forces between a mica substrate and the same sphere are as large as 10 μN deeming contact measurements with soft cantilevers (spring constant < 1 N/m) even impossible since the retraction range is outside of that of most piezo z-ranges. Measurements of the capillary forces with a smooth sphere used for the Casimir force measurement are shown in Fig. 11. One can see that when roughness increases a few times the force decreases by more than a factor of 100. This can be related to full sphere wetting and asperity wetting. The size of the sphere $R = 50\,\mu$m

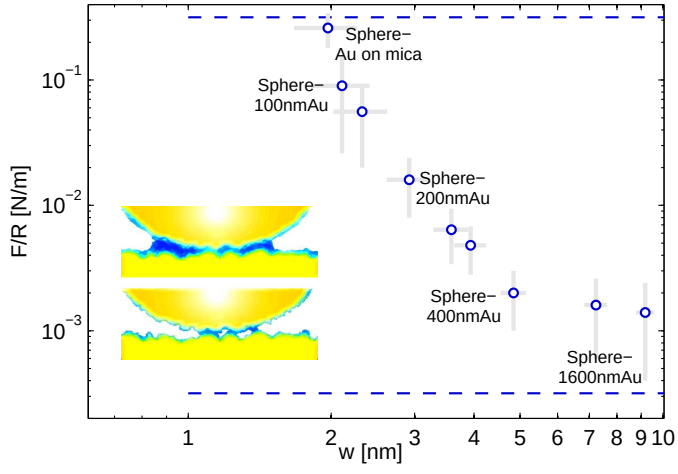

Fig. 11 Capillary forces in air (relative humidity 2-60%) for a smooth gold coated sphere, $w_{sph} \sim 1$ nm, measured with a stiff cantilever, $k = 4$ N/m, and different rough films. The inset shows a fully wetted sphere (upper dashed line), and a roughness asperity wetted sphere (lower dashed line).

is 1000 times larger than that of an asperity $\xi \sim 50$ nm. Multiple asperity capillary bridge formation is likely to happen in the rough regime giving increasing forces.

Furthermore, formation of capillary bridges means that under ambient conditions gold absorbs water, and as a result it is covered with an ultra thin water layer. The experiments [69, 67] suggest that the thickness of this layer is in the nanometer range, 1-2 nm. The natural questions one could ask is how thick the water layer is, and what is the influence of this water layer on the dispersive force [71]? At short separations, $d < 20$ nm, these questions become of crucial importance because they place doubts in our understanding of the dispersive forces when experiments under ambient conditions are compared with predictions of the Lifshitz theory. Figure 12 shows the Casimir force measured at short distances together with theoretical calculations made for gold with or without a water layer on top. The errors are shown to arise mainly from the experimental uncertainty in determining the separation upon contact d_0 due to nanoscale surface roughness. We can conclude that the experiment can exclude the water layer thicker than 1.5 nm. Figure 12(b) shows that the effect of water becomes very significant at separations below 10 nm, which were not accessible in our measurements due to jump-into-contact. We presented only the forces between flat surfaces because at these small separations there is no a reliable way to estimate the roughness correction.

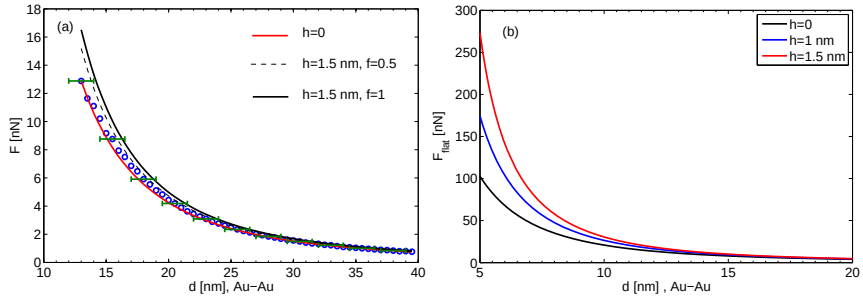

Fig. 12 (a) Experimental data for the force vs distance (circles) down to 13 nm separations, and the theoretical prediction without water layer (red curve). Errors in the absolute separation are shown for some points by the bars. The continuous black curve is the prediction for continuous water layer of thickness $h = 1.5$ nm. The dashed black curve corresponds to the same water layer with 50% of voids ($f = 0.5$). (b) Theoretical calculations using the Lifsthiz theory for flat surfaces and continuous water layer films with thicknesses h =0, 1, 1.5 nm for small separations.

3.3 Distance upon contact

The absolute distance separating two bodies is a parameter of principal importance for the determination of dispersive forces. It becomes difficult to determine when the separation gap approaches nanometer dimensions. This complication originates from the presence of surface roughness, which manifests itself on the same scale. In fact, when the bodies are brought into gentle contact they are still separated by some distance d_0, which we call the distance upon contact due to surface roughness. This distance has a special significance for weak adhesion, which is mainly due to van der Waals forces across an extensive noncontact area [21]. It is important for MEMS and NEMS as unremovable reason for stiction [22]. In the modern precise measurements of the dispersive forces d_0 is the main source of errors (see reviews [5, 6]). This parameter is typically determined using electrostatic calibration. The distance upon contact is usually considerably larger than the rms roughness because it is defined by the highest asperities. It is important to clear understand the origin of d_0, its dependence on the lateral size L of involved surfaces, and possible uncertainties in its value [72]. These are the questions we address in this subsection.

3.3.1 Plate-plate contact

Two plates separated by the distance d and having roughness profiles $h_i(x,y)$ locally are separated by the distance $d(x,y)$ given by Eq. (25) (see Fig. 9). Indeed, the averaged local distance has to give d, $\langle d(x,y)\rangle = d$. We can define the distance upon contact d_0 as the largest distance $d = d_0$, for which $d(x,y)$ becomes zero.

It is well known from contact mechanics [73] that the contact of two elastic rough plates is equivalent to the contact of a rough hard plate and an elastic flat plate with an effective Young's modulus E and a Poisson ratio ν. Here we analyze the contact in the limit of zero load when both bodies can be considered as hard. This limit is realized when only weak adhesion is possible, for which the dispersive forces are responsible. Strong adhesion due to chemical bonding or due to capillary forces is not considered here. This is not a principal restriction, but the case of strong adhesion has to be analyzed separately. Equation (25) shows that the profile of the effective rough body is given by

$$h(x,y) = h_1(x,y) + h_2(x,y). \tag{28}$$

The latter means that $h(x,y)$ is given by the combined image of the surfaces facing each other. If topography of the surfaces was determined with AFM, we have to take the sum of these two images and the combined image will have the size of the smallest image.

To determine d_0 we collected [72] high resolution megascans (size $40\times 40\ \mu\text{m}^2$, lateral resolution 4096×4096 pixels) for gold films of different thicknesses described before. The maximal area, which we have been able to scan on the sphere, was $8\times 8\ \mu\text{m}^2$ (2048×2048 pixels). The images of 100 nm film, sphere, and 1600 nm film are shown in Fig. 1 (a), (b), and (c), respectively. Combining two images and calculating from them the maximal peak height we can find d_0 for a given size of the combined image. Of course, taking the images of the same size every time we will get different value of d_0 and averaging over a large number of images we will find the averaged d_0 and possible rms deviations. This is quite obvious. What is less obvious is that if we take images of different size and will do the same procedure the result for d_0 will be different.

Let L_0 be the size of the combined image. Then, in order to obtain information on the scale $L = L_0/2^n$, we divide this image on 2^n subimages. For each subimage we find the highest point of the profile (local d_0), and average all these values. This procedure gives us $d_0(L)$ and the corresponding statistical error. Megascans are very convenient for this purpose otherwise one has to collect many scans in different locations. For the 100 nm film above the 400 nm film the result of this procedure is shown in Fig. 13(a). We took the maximum area to be $10\times 10\ \mu\text{m}^2$. The figure clearly demonstrates the dependence of d_0 on the scale L although the errors appear to be significant. The dependence of the rms roughness w on the length scale L is absent in accordance with the expectations, while only the error bars increase when L is decreasing.

To understand the dependence $d_0(L)$ let us assume that the size L of the area of nominal contact is large in comparison with the correlation length, $L \gg \xi$. It means that this area can be divided into a large number $N^2 = L^2/\xi^2$ of cells. The height of each cell (asperity) can be considered as a random variable h. The probability to find h smaller than some value z can be presented in a general form

$$P(z) = 1 - e^{-\phi(z)}, \tag{29}$$

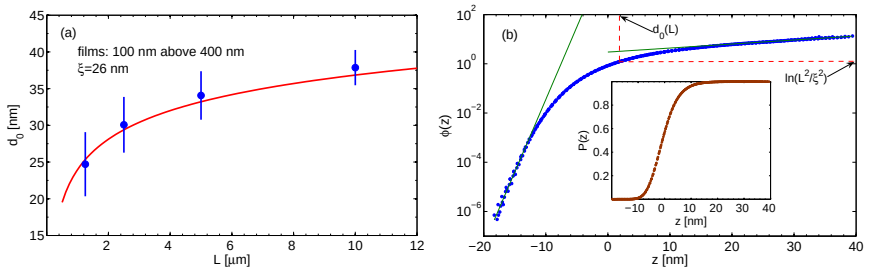

Fig. 13 (a) Distance upon contact as a function of the length scale. Dots with the error bars are the values calculated from the megascans. The solid curve is the theoretical expectation according to Eq. (30). Note that d_0 is considerably larger than w. (b) Statistics of the surface roughness. Four 10×10 μm^2 images were used. The main graph shows the "phase" as a function of z. The green lines show the best fits at large positive and negative z. The dashed red lines demonstrate the solution of Eq. (30). The inset shows the cumulative distribution $P(z)$.

where the "phase" $\phi(z)$ is a nonnegative and nondecreasing function of z. Note that (29) is just a convenient way to represent the data: instead of cumulative distributions $P(z)$ we are using the phase $\phi(z)$, which is not so sharp function of z.

For a given asperity the probability to find its height above d_0 is $1-P(d_0)$, then within the area of nominal contact one asperity will be higher than d_0 if

$$e^{-\phi(d_0)}\left(L^2/\xi^2\right) = 1 \quad \text{or} \quad \phi(d_0) = \ln\left(L^2/\xi^2\right). \tag{30}$$

This condition can be considered as an equation for the asperity height because due to a sharp exponential behavior the height is approximately equal to d_0. To solve (30) we have to know the function $\phi(z)$, which can be found from the roughness profile.

The cumulative distribution $P(z)$ can be extracted from combined images by counting pixels with the height below z. Then the "phase" is calculated as $\phi(z) = -\ln(1-P)$. The results are presented in Fig. 13(b). The procedure of solving Eq. (30) is shown schematically in Fig. 13(b) by dashed red curves, and the solution itself is the red curve in Fig. 13(a). It has to be mentioned that the normal distribution fails to describe the data at large z. Other known distributions cannot satisfactory describe the data for all z. Asymptotically at large $|z|$ the data can be reasonably well fit with the generalized extreme value Gumbel distributions (green lines in Fig. 13(b)) [74]:

$$\ln\phi(z) = \begin{cases} -\alpha z, & z \to -\infty \\ \beta z, & z \to \infty \end{cases} \tag{31}$$

The observed dependence $d_0(L)$ can be understood intuitively. The probability to have one high asperity is exponentially small but the number of asperities increases with the area of nominal contact. Therefore, the larger the contact area, the higher probability to find a high feature within this area. Scale dependence of d_0 shows that smaller areas getting into contact will be bound more strongly than larger areas

because upon the contact they will be separated by smaller distances. This fact is important for weak adhesion analysis.

3.3.2 Sphere-plate contact

Most of the Casimir force experiments measure the force in the sphere-plate configuration to avoid the problem with the plates parallelism. Let us consider how the scale dependence of d_0 manifests itself in this case. Assuming that the sphere is large, $R \gg d$, the local distance is

$$d(x,y) = d + \left(x^2 + y^2\right)/2R - h(x,y), \tag{32}$$

where $h(x,y)$ is the combined topography of the sphere and the plate. As in the plate-plate case d_0 is the maximal d, for which the local distance becomes zero. This definition gives

$$d_0 = \max_{x,y} \left[h(x,y) - \left(x^2 + y^2\right)/2R\right]. \tag{33}$$

Now d_0 is a function of the sphere radius R, but, of course, one can define the length scale L_R corresponding to this radius R.

As input data in Eq. (33) we used the combined images of the sphere and different plates. The origin ($x = 0$, $y = 0$) was chosen randomly in different positions and then d_0 was calculated according to (33). We averaged d_0 found in 80 different locations to get the values of d_0^{im}, which are collected in Tab. 3. The same values can be determined theoretically using $d_0(L)$ found between two plates (see Eq. (30) and Ref. [72]).

	100 *nm*	200 nm	400 nm	800 nm	1600 nm
w	3.8	4.2	6.0	7.5	10.1
ξ	26.1(3.8)	28.8(3.7)	34.4(4.7)	30.6(2.4)	42.0(5.5)
d_0^{im}	12.8(2.2)	15.9(2.7)	24.5(4.8)	31.3(5.4)	55.7(9.3)
d_0^{el}	17.7(1.1)	20.2(1.2)	23.0(0.9)	34.5(1.7)	50.8(1.3)

Table 3 The parameters characterizing the sphere-film systems (all in nm) for $R = 50$ μm. The first three rows were determined from combined images. The last row for d_0^{el} gives the values of d_0 determined electrostatically. The errors are indicared in brackets.

The values of d_0^{im} for rougher films are in agreement with those found from the electrostatic calibration. However, for smoother films (100 and 200 nm) d_0^{im} and d_0^{el} do not agree with each other. This is most likely to be attributed to the roughness on the sphere, which varies considerably locally. For example, between those 80 d_0^{im} found in different locations 5% are in agreement with d_0^{el} found from the electrostatic calibration [72]. This is illustrated by the fact that when the roughness of the plate dominates the discrepancy between d_0^{im} and d_0^{el} disappears. Note that the

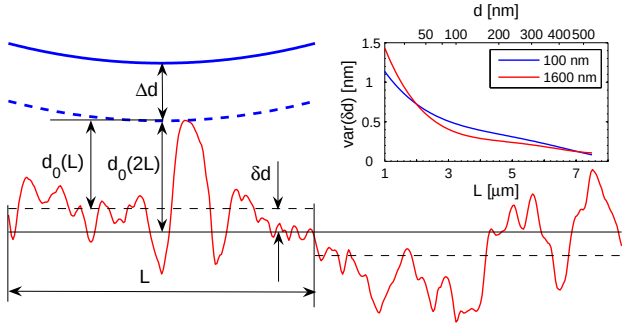

Fig. 14 Schematic explanation of additional uncertainty δd in d_0 (see text). The sphere in two positions is shown by the dashed (contact) and solid blue curves. The inset shows the variance of δd as a function of the scale L or separation d.

standard deviations for d_0^{im} are larger than that for d_0^{el}. The standard deviations in d_0^{im} originate from place to place variations of d_0^{im}. In the case of electrostatic determination of d_0 statistical variation of d_0 from place to place is not included in the errors of d_0^{el}. This explains why the errors in d_0^{el} are smaller.

Consider the experimental situation when the dispersive force is measured in the sphere-plate configuration. The system under consideration is equivalent to a smooth sphere above a combined rough profile $h(x,y)$. The position of the average plane depends on the area of averaging L^2 especially for small scales L. The profile shown in Fig. 14 demonstrates different mean values in the left and right segments shown by the dashed black lines. Both of these values deviate from the middle line for the scale $2L$ (solid black line). The true average plane is defined for $L \to \infty$.

Position of the average plane define the absolute separation of the bodies. It has to be stressed that the electrostatic and Casimir interactions "see" different areas on the plate. This is due to different dependence on d and quite often the electrostatic calibration is performed at larger separations than measurement of the Casimir force. The size L of the interaction area is determined by the relation $L^2 = \alpha\pi Rd$, where $\alpha = 2$ for the electrostatic and $\alpha = 2/3$ for pure Casimir force. Therefore, these two interactions can "see" different positions of the average planes. It introduces an additional uncertainty δd in the absolute separation [72]. For a fixed L this uncertainty is a random variable distributed roughly normally around $\delta d = 0$. However, it has to be stressed that δd manifests itself not as a statistical error but rather as a kind of a systematic error. This is because at a given lateral position of the sphere this uncertainty takes a fixed value. The variance of δd is defined by the roughness statistics. It was calculated from the images and shown as inset in Fig. 14. One has to remember that with a probability of 30% the value of δd can be larger than that shown in Fig. 14.

4 Conclusions

In this chapter we considered the Casimir force between realistic materials containing defects, which influence the optical properties of interacting materials, and having surface roughness, which contributes to the force.

It was demonstrated that the gold films prepared in different conditions have dielectric functions, which differ from sample to sample, and this difference cannot be ignored in the calculation of the Casimir force aimed at precision better than 10%. The main conclusion is that for metals one has to measure the dielectric function of used materials in a wide range of frequencies, where far and mid IR are especially important. Precise knowledge of the dielectric functions is also important for low dielectric materials. In this case significant sensitivity of the force to the dielectric functions is realized nearby the attractive-to-repulsive transition in solid-liquid-solid systems.

The roughness correction to the Casimir force can be reliably calculated if rms roughness w is small in comparison with the separation, $w \ll d$, when one can apply the perturbation theory. In the experiments at short separations this condition can be violated. The current situation with the theory is that there is no direct method to calculate the force between rough bodies when $d \sim w$ except using rather complicated numerical calculations.

We gave also a detailed analysis of the distance upon contact, d_0, which is an important parameter in Casimir physics. Analysis of AFM scans demonstrated that d_0 is always a few times larger than the rms roughness. Moreover, d_0 is a function of the size L of the nominal area of contact. This dependence is important for weak adhesion, which is due to van der Waals forces across an extensive noncontact area. Uncertainty in d_0 is the main source of errors in the Casimir force measurements. We demonstrated here that there is an additional indefiniteness in d_0, which cannot be excluded by the electrostatic calibration. It becomes very important for small areas of interaction. Also, this indefiniteness has to be taken into account if one compares two independent experiments.

Acknowledgements The research was carried out under Project No. MC3.05242 in the framework of the Strategic Research Programme of the Materials Innovation Institute M2i (the former Netherlands Institute for Metals Research NIMR) The authors benefited from exchange of ideas by the ESF Research Network CASIMIR.

References

1. Casimir, H. B. G.: On the attraction between two perfectly conducting plates. Proc. K. Ned. Akad. Wet. **51**, 793–795 (1948)
2. Lifshitz, E. M. , Zh. Eksp. Teor. Fiz. **29**, 894 (1955) [Soviet Phys. JETP **2**, 73 (1956)]
3. Dzyaloshinskii, I. E., Lifshitz, E. M., Pitaevskii, L. P.: General theory of van der Waals' forces. Usp. Fiz. Nauk **73**, 381–421 (1961) [Soviet Phys. Usp. **4**, 153–176 (1961)]
4. Lifshitz, E. M., Pitaevskii, L. P.: Statistical Physics, Part 2. Pergamon, Oxford (1980)

5. Lamoreaux, S. K.: The Casimir force: background, experiments, and applications. Rep. Prog. Phys. **68**, 201–236 (2005)
6. Capasso, F., Munday, J. N., Iannuzzi, D., Chan, H. B.: Casimir Forces and Quantum Electrodynamical Torques: Physics and Nanomechanics. IEEE J. Sel. Top. Quantum Electron. **13**, 400–414 (2007)
7. Palik, E. D.: Handbook of Optical Constants of Solids. Academic Press, (1995)
8. Weaver, J. H., Krafka, C., Lynch, D. W., Koch, E. E.: Optical Properties of Metals, Part II, Physics Data No. 18-2. Fachinformationszentrum Energie, Physik, Mathematik, Karsruhe, (1981)
9. Lambrecht, A., Reynaud, S.: Casimir force between metallic mirrors. Eur. Phys. J. D **8**, 309–318 (2000)
10. Lamoreaux, S. K.: Calculation of the Casimir force between imperfectly conducting plates. Phys. Rev. A **59**, R3149–R3153 (1999)
11. Lamoreaux, S. K.: Comment on "Precision Measurement of the Casimir Force from 0.1 to 0.9 μm". Phys. Rev. Lett. **83**, 3340 (1999)
12. Svetovoy, V. B., Lokhanin, M. V.: Do the precise measurements of the Casimir force agree with the expectations? Mod. Phys. Lett. A **15**, 1013–1021 (2000)
13. Svetovoy, V. B., Lokhanin, M. V.: Precise calculation of the Casimir force between gold surfaces. Mod. Phys. Lett. A **15**, 1437–1444 (2000)
14. Pirozhenko I., Lambrecht A., Svetovoy, V.B.: Sample dependence of the Casimir force. New J. Phys. bf 8 238 (2006)
15. Svetovoy, V. B., van Zwol, P. J., Palasantzas, G., De Hosson, J. Th. M.: Optical properties of gold films and the Casimir force. Phys. Rev. B **77**, 035439 (2008)
16. van Zwol, P. J., Palasantzas, G., De Hosson, J. Th. M.: Influence of dielectric properties on van der Waals/Casimir forces in solid-liquid systems. Phys. Rev. **79**, 195428 (2009)
17. Genet, C., Lambrecht, A., Maia Neto, P., Reynaud, S.: The Casimir force between rough metallic plates. Europhys. Lett. **62**, 484–490 (2003)
18. Maia Neto, P., Lambrecht, A., Reynaud, S.: Roughness correction to the Casimir force: Beyond the Proximity Force Approximation. Europhys. Lett. **69**, 924–930 (2005)
19. Maia Neto, P., Lambrecht, A., Reynaud, S.: Casimir effect with rough metallic mirrors. Phys. Rev. A **72**, 012115 (2005)
20. Derjaguin, B. V., Abrikosova, I. I., Lifshitz, E. M. : Direct measurement of molecular attraction between solids separated by a narrow gap. Q. Rev. Chem. Soc. **10**, 295–329 (1956)
21. DelRio, F. W., de Boer, M. P., Knapp, J. A., Reedy Jr, E. D., Clews, P. J., Dunn, M. L.: The role of van derWaals forces in adhesion of micromachined surfaces. Nat. Mater. **4**, 629–634 (2005)
22. Maboudian, R., Howe, R. T.: Critical review: Adhesion in surface micromechanical structures. J. Vac. Sci. Technol. B **15**, 1 (1997)
23. Houston, M. R., Howe, R. T., Maboudiana, R.: Effect of hydrogen termination on the work of adhesion between rough polycrystalline silicon surfaces. J. Appl. Phys. **81**, 3474–3483 (1997)
24. van Zwol, P. J., Palasantzas, G., De Hosson, J. Th. M.: Influence of random roughness on the Casimir force at small separations. Phys. Rev. B **77**, 075412 (2008)
25. Lamoreaux, S. K.: Demonstration of the Casimir force in the 0.6 to 6 μm range. Phys. Rev. Lett. **78**, 5–8 (1997)
26. Harris, B.W. et. al.: Precision measurement of the Casimir force using gold surfaces. Phys. Rev. A. **62**, 052109 (2000)
27. Decca, R. S. et al.: Tests of new physics from precise measurements of the Casimir pressure between two gold-coated plates. Phys. Rev. D **75**, 077101 (2007)
28. Aspnes, D. E., Kinsbron, E., Bacon, D. D.: Optical properties of Au: Sample effects. Phys. Rev B **21**, 3290–3299 (1980)
29. Chen, F., Mohideen, U., Klimchitskaya, G.L., Mostepanenko, V.M.: Investigation of the Casimir force between metal and semiconductor test bodies. Phys. Rev. A **72**, 020101 (2005)
30. Dold, B., Mecke, R.: Optische Eigenschaften von Edelmetallen, Übergangsmetallen und deren Legierungen im Infratot. Optik, **22**, 435–446 (1965).

31. Motulevich, G. P., Shubin, A. A.: Influence of Fermi surface shape in gold on the optical constants and Hall effect. Zh. Eksp. Teor. Fiz. **47**, 840 (1964) [Soviet Phys. JETP **20**, 560–564 (1965)].
32. Landau, L. D., Lifshitz, E. M.: Electrodynamics of Continuous Media. Pergamon Press, Oxford (1963)
33. Zhou, F., Spruch, L.: van der Waals and retardation (Casimir) interactions of an electron or an atom with multilayered walls. Phys. Rev. A **52**, 297–310 (1995)
34. Iannuzzi, D., Lisanti, M., Capasso, F.: Effect of hydrogen-switchable mirrors on the Casimir force. Proc. Natl. Acad. Sci. U.S.A. **101**, 4019-4023 (2004)
35. Lisanti, M., Iannuzzi, D., Capasso, F.: Observation of the skin-depth effect on the Casimir force between metallic surfaces. Proc. Natl. Acad. Sci. U.S.A. **102**, 11989-11992 (2005)
36. de Man, S., Heeck, K., Wijngaarden, R. J., Iannuzzi, D.: Halving the Casimir force with Conductive Oxides. Phys. Rev. Lett. **103**, 040402 (2009)
37. Azzam, R. M. A., Bashara N. M.: Ellipsometry and Polarized Light. North Holland, Amsterdam (1987)
38. Tompkins, H. G., McGahan, W. A.: Spectroscopic Ellipsometry and Reflectometry. Wiley, New York (1999)
39. Hofmann, T. et. al.: Terahertz Ellipsometry Using Electron-Beam Based Sources. Mater. Res. Soc. Symp. Proc. **1108**, A08-04 (2009)
40. Feng, R., Brion C. E.: Absolute photoabsorption cross-sections (oscillator strengths) for ethanol (5 – 200 eV). Chem. Phys. **282**, 419–427 (2002)
41. Tompkins, H. G., Irene, E. A.: Handbook of ellipsometry William Andrew (2005)
42. van Zwol, P. J., Palasantzas, G., van de Schootbrugge, M., De Hosson, J. Th. M.: Measurement of dispersive forces between evaporated metal surfaces in the range below 100 nm. Appl. Phys. Lett. **92**, 054101 (2008)
43. http://www.JAWoollam.com
44. Thèye, M.-L.: Investigation of the Optical Properties of Au by Means of Thin Semitransparent Films. Phys. Rev. B **2**, 3060-3078 (1970)
45. Munday, J. N., Capasso, F., Parsegian, A.: Measured long-range repulsive CasimirLifshitz forces. Nature **457**, 170–173 (2009)
46. Dagastine, R. R., Prieve, D. C., White L. R.: The Dielectric Function for Water and Its Application to van der Waals Forces. J. Colloid Interface Sci. **231**, 351–358 (2000)
47. Munday, J. N., Capasso, F., Parsegian, A., Bezrukov, S. M.: Measurements of the Casimir-Lifshitz force in fluids: The effect of electrostatic forces and Debye screening. Phys. Rev. A **78**, 032109 (2008)
48. Kitamura R. et. al.: Optical constants of silica glass from extreme ultraviolet to far infrared at near room temperature. Appl. Optics **46**, 8118 (2007)
49. Segelstein, D. J.: The Complex Refractive Index Of Water. PhD thesis, University of Missouri: Kansas City, USA (1981)
50. Nguyen, A. V.: Improved approximation of water dielectric permittivity for calculation of hamaker constants. J. Colloid Interface Sci. **229**, 648–651 (2000)
51. Parsegian, V. A., Weiss, G. H.: Spectroscopic parameters for computation of van der Waals forces. J. Colloid Interface Sci. **81**, 285-289 (1981)
52. Roth, C. M., Lenhoff, A. M.: Improved parametric representation of water dielectric data for Lifshitz theory calculations. J. Colloid Interface Sci. **179**, 637–639 (1996)
53. van Oss, C. J., Chaudhury, M. K., Good, R. J.: Interfacial Lifshitz-van der Waals and polar interactions in macroscopic systems. Chem. Rev. **88**, 927-941 (1988)
54. Milling, A., Mulvaney, P., Larson, I.: Direct measurement of repulsive van der Waals interactions using an atomic force microscope. J. Colloid Interface Sci. **180**, 460465 (1996).
55. Ogawa, M., Cook, G. R.: Absorption Coefficients of Methyl, Ethyl, N-Propyl and N-Butyl Alcohols. J. Chem. Phys **28** 747–748 (1957)
56. Salahub, D. R., Sandorfy, C.: The far-ultraviolet spectra of some simple alcohols and fluoroalcohols. Chem. Phys. Lett. **8**, 71–74 (1971)
57. Koizumi H. et. al.: VUV-optical oscillator strength distributions of C_2H_6O and C_3H_8O isomers. J. Chem. Phys. **85** 4276–4279 (1986)

58. Sethna, P. P., Williams, D.: Optical constants of alcohols in the infrared. J. Phys. Chem. **83** , 405–409 (1979)
59. Bertie, J. E., Zhang, S. L., Keefe, C. D.: Measurement and use of absolute infrared absorption intensities of neat liquids. Vibrational Spectroscopy **8** 215-229 (1995)
60. van Zwol, P. J., Palasantzas, G., DeHosson, J. Th. M.: Weak dispersion forces between glass and gold macroscopic surfaces in alcohols. Phys. Rev. E. **79**, 041605 (2009)
61. Meakin, P.: The growth of rough surfaces and interfaces. Phys. Rep. **235**, 189–289 (1993)
62. Palasantzas, G., Krim, J.: Experimental Observation of Self-Affine Scaling and Kinetic Roughening at Sub-Micron Lengthscales. Int. J. Mod. Phys. B, **9** 599–632 (1995)
63. Zhao, Y., Wang, G.-C., Lu, T.-M.: Characterization of amorphous and crystalline rough surfaces-principles and applications. Academic Press (2001)
64. Palasantzas, G.: Power spectrum and surface width of self-affine fractal surfaces via the k-correlation model. Phys. Rev. B **48**, 14472–14478 (1993); **49**, 5785 (1994)
65. Klimchitskaya, G. L., Pavlov, Yu. V.: The correction to the Casimir forces for configurations used in experiments: the spherical lens above the plane and two crossed cylinders. Int. J. Mod. Phys. A **11**, 3723–3742 (1996).
66. Rodriguez, A., Ibanescu, M., Iannuzzi D., Capasso, F., Joannopoulos, J. D., Johnson, S. G.: Computation and Visualization of Casimir Forces in Arbitrary Geometries: Nonmonotonic Lateral-Wall Forces and the Failure of Proximity-Force Approximations. Phys. Rev. Lett. **99**, 080401 (2007)
67. van Zwol, P. J., Palasantzas, G., De Hosson, J. Th. M.: Influence of roughness on capillary forces between hydrophilic sur-faces. Phys. Rev. E **78**, 031606 (2008)
68. DelRio, F. W., Dunn, M. L., Phinney, L. M., Bourdon, C. J.: Rough surface adhesion in the presence of capillary condensation. Appl. Phys. Lett. **90**, 163104 (2007)
69. van Zwol, P. J., Palasantzas, G., De Hosson, J. Th. M.: Influence of random roughness on the adhesion between metal surfaces due to capillary condensation. Appl. Phys. Lett. **91**, 101905 (2007)
70. Israelachvili, J.: Intermolecular and surface forces. Academic, New York (1992)
71. Palasantzas, G., Svetovoy, V. B., van Zwol, P. J.: Influence of water adsorbed on gold on van der Waals/Casimir forces. Phys. Rev. B **79**, 235434 (2009)
72. van Zwol, P. J., Svetovoy, V. B., Palasantzas, G.: Distance upon contact: Determination from roughness profile. Phys. Rev. B **80**, 235401 (2009)
73. Greenwood, J. A., Williamson, J. B. P.: Contact of nominally flat surfaces. Proc. R. Soc. A **295**, 300–319 (1966)
74. Coles, S.: An introduction to statistical modelling of extreme values. Springer, Berlin (2001)